atmosphere

MDPI

Article

Parallel Surface Renewal for Estimating Turbulent Fluxes in Vineyards and Almond Orchards

Francesc Castellví [1,*], Juan M. Sánchez [2] and Ramón López-Urrea [3]

[1] Department of Chemist, Physics, Environment and Soil Sciences, University of Lleida, 25003 Lleida, Spain
[2] Department of Physics, University of Castilla-La Mancha, Remote Sensing, Agronomy and Irrigation, Associated Unit to CSIC by CIDE, Campus Universitario, 02071 Albacete, Spain; juanmanuel.sanchez@uclm.es
[3] Desertification Research Centre (CIDE), CSIC-UV-GVA, Ctra CV 315, Km 10.7, 46113 Moncada, Valencia, Spain; lopez-urrea@csic.es
* Correspondence: francesc.castellvi@udl.cat

Abstract

The La Mancha region (a semi-arid area of southeast Spain) hosts the world's highest concentration of vineyards and is also one of the regions with the largest areas devoted to almond tree cultivation. Viticulture and nut fruit trees (mainly almonds) are one of the region's principal sources of economic revenue. The Two-Source Energy Balance (TSEB) model can assist management of water resources. A simplified version of the TSEB approach (STSEB) was previously tested in a vineyard and almonds to estimate sensible heat (H) and latent heat (LE) fluxes using a parallel scheme method based on the Monin–Obukov similarity theory (MOST). This study introduces a method based on Surface Renewal (SR) theory to partition the sensible heat flux using low-frequency measurements as input. The latter was friendlier than the parallel MOST method under unstable conditions and than the series SR and MOST methods. The objective was to compare the MOST and SR models within a parallel scheme method. During the 2014 and 2015 growing season, measurements were collected in a 4 ha row crop drip-irrigated Tempranillo vineyard. Hourly sensible heat flux measured by an eddy covariance (EC) system and evapotranspiration (ET) registered by a 9 m^2 monolithic large weighting lysimeter were used as a reference. ET estimates were obtained as a residual of the energy balance equation (known as the residual method) using three methods for estimating sensible heat flux, H_{SR}, H_{MOST} and H_{EC}, yielding $ET_{SR\text{-}RE}$, $ET_{MOST\text{-}RE}$ and $ET_{EC\text{-}RE}$, respectively. For sensible heat flux, the index of agreement (IA expressed in %) for 2014 and 2015 was 93% and 83%, respectively, using SR, and 84% and 78%, respectively, for MOST. This represents a 6–10% improvement using SR. For evapotranspiration, the $ET_{SR\text{-}RE}$ and $ET_{MOST\text{-}RE}$ IA showed similar performance in both years (around 88%), while $ET_{EC\text{-}RE}$ yielded the best results (92% and 89% for 2014 and 2015, respectively). In addition, half-hourly EC fluxes, during the growing season of 2017, were used as a reference in an almond orchard. The SR sensible heat flux performed better (IA = 93%) than MOST (IA = 86%) in this case, whereas for the latent heat flux, the residual method performed the best, resulting in an IA of 81% for SR and of 78% for MOST. Overall, SR performed better than MOST, particularly under unstable conditions with wind speeds above 1 ms^{-1}.

Keywords: sensible heat flux; latent heat flux; eddy covariance system; large weighing lysimeter; crop evapotranspiration

Check for updates

Academic Editor: Stephan De Wekker

Received: 28 April 2026
Revised: 1 June 2026
Accepted: 6 June 2026
Published: 9 June 2026

Copyright: © 2026 by the authors. Licensee MDPI, Basel, Switzerland. This article is an open access article distributed under the terms and conditions of the Creative Commons Attribution (CC BY) license.

1. Introduction

Given the current climate change conditions, reducing uncertainty in the estimation of actual crop evapotranspiration (ET) is critical to achieve a more effective irrigation scheduling of croplands [1–3]. Thus, irrigation must be carefully managed to prevent severe water stress in regions with scarce water resources [4–6]. The present work focuses on irrigated wine grapes and almond trees under semi-arid conditions, where ET plays a significant role. The experiments were conducted in the Castilla—La Mancha region (Spain), where water requirements are highest in summer, evaporative demand is high, and rainfall is scarce. Annual rainfall varies from 250 to 350 mm; irrigation is expanding year on year; and population and industrial growth are increasing. In this scenario, optimizing the management of water resources becomes crucial.

As in most models in eco-hydrological studies, latent heat flux (LE) is estimated as the residual calculation from the simplified surface energy balance equation, which includes net radiation (R_n), soil heat flux (G), and sensible heat flux (H); thus, LE = $R_n - G - H$. The residual technique assumes H is accurate. For sparse vegetation, assuming that the net surface energy, ($R_n - G$), is known, various methods and techniques for partitioning and estimating sensible heat flux have been applied to determine actual water use, e.g., [7–15], among many others. For micrometeorologists, eddy covariance (EC) is the prevalent technique for ground measuring ET (i.e, LE converted to ET). However, the EC turbulent fluxes are typically underestimated [16,17]. For agronomists, the weighing lysimeter is the benchmark for direct ET measurement, but only if the fundamental criteria for the representativeness of vegetation and environmental conditions are satisfied [1,18–21]. For sparse canopies, a series scheme of the surface renewal (SR) model for estimating the partitioning of sensible heat flux was used within the Two-Source Energy Balance (TSEB) framework [22]. The methodology for estimating the partitioning of the latent heat flux, the radiation, and the soil heat flux was that used in the original TSEB method [23]. Estimation of sensible heat flux using TSEB is based on the Monin–Obukov similarity theory (MOST) which has been extensively applied in series and parallel schemes. The Simplified Two-Source Energy Balance (STSEB) model for estimating sensible heat flux uses a parallel scheme, and the objective was to compare this versus SR applied in parallel. The parallel SR method was friendlier than the series SR and MOST methods because they need to compute the temperature in the canopy air space [3,9,22]. Also, for estimating the sensible heat flux, it is more direct than the parallel MOST method under unstable conditions [24]. For estimating the soil heat flux, the SR method set the roughness length for momentum to 0.004 m (aan intermediate value for bare soils) as a default. However, the latter can be conventionally estimated depending on the soil type and the land uses requiring site-specific calibration.

Hereinafter, the sensible heat flux and the latent heat flux estimated using SR and MOST combined with STSEB are denoted H_{SR}, H_{MOST}, LE_{SR}, LE_{MOST}, respectively. Assuming that the estimated net surface energy balance, $(R_n - G)_{Est}$, is known, LE determined using the residual method (RE) is denoted $LE_{SR\text{-}RE} = (R_n - G)_{Est} - H_{SR}$ and $LE_{MOST\text{-}RE} = (R_n - G)_{Est} - H_{MOST}$, and the ET as $ET_{SR\text{-}RE}$ and $ET_{MOST\text{-}RE}$ for SR and MOST methods, respectively.

In 2014 and 2015, an experiment was conducted in a 4 ha Tempranillo vineyard to validate modeled ET against lysimeter observations [7]. A surface energy imbalance close to 27% was reported on an hourly basis (according to the lysimeter output). These authors found improved agreement with the lysimeter registers, ET_{Lys}, when the residual approach was applied using $ET_{EC\text{-}RE} = R_n - G - H_{EC}$. The reported agreement between $ET_{EC\text{-}RE}$ and ET_{Lys} (RMSE ~0.09 mm h^{-1}) supports the validity of both methods to compare the ET estimates in the experiment. Therefore, the hourly H_{EC} and ET_{Lys} were used as a reference.

In 2017, the experiment focused on an 11 ha young almond orchard. The EC technique was used for estimating the half-hourly sensible and latent heat fluxes. Here, an acceptable closure of the surface energy balance of $(Rn - G - H_{EC} - LE_{EC}) \geq 0.8$ was obtained [16]. All the data available were for unstable conditions.

2. Materials and Methods

2.1. Study Site and Measurements

A detailed description of the study sites and materials is available in [7,25]. The monthly weather data from a nearby agro-meteorological station located in Albacete, (southeast Spain) were analyzed for a 30-year period (1987–2016). The climograph showed that for the four months from June to September, the site was arid, and the two from July to August were dry, with monthly precipitation being below 30 mm. The mean annual precipitation was 314 mm, mostly concentrated during spring and autumn. The mean monthly maximum and minimum air temperatures were 24.7 °C and 4.8 °C, respectively, and the mean daily wind speed was 2.5 m s^{-1}. The climate in this area is inland Mediterranean with warm summers characterized by dry and hot atmospheric conditions and clear days. For both campaigns, the weather observed during the experiment was typical of the semi-arid climate of Central Spain.

2.1.1. Vineyard

The experiment was conducted on Tempranillo grapevines (*Vitis vinifera* L., cv. Tempranillo) during the 2014 and 2015 growing seasons at a site located at 39°3′ N, 2°5′ W, and 695 m a.s.l. The dataset included 76 days in 2014 (DOYs 170–246) and 113 days in 2015 (DOYs 183–296). Throughout the study period, accumulated rainfall reached 34.4 mm in 2014, mainly concentrated on 22 and 24 June, whereas in 2015, cumulative precipitation was 65.4 mm, mostly occurring during late summer.

The vineyard occupied an area of 4 ha and was oriented west–east, forming an angle of 70° with respect to the north. Vine spacing within rows was 1.5 m, while row spacing was 3 m. Vines were trained on a vertical trellis system, with a canopy height of approximately 1.5 m. The soil was of a silty–clay–loam texture, composed of 13% sand, 49% silt, and 38% clay, and presented a basic pH.

Sensible heat flux and evapotranspiration (ET) were determined on an hourly basis. Crop ET was measured using a monolithic large weighing lysimeter consisting of a 3 m × 3 m container with a depth of 1.7 m, providing a resolution equivalent to 0.03 mm of water depth. The installation site and maintenance conditions of the lysimeter fulfilled the standards required to ensure representative ET measurements [18], including a minimum fetch distance of 50 m surrounding the lysimeter location. Soil water conditions within the lysimeter were maintained under non-limiting conditions. During 2014, the system received 22 irrigation events with a total applied irrigation water (AIW) of 202 mm, whereas in 2015 a total of 42 irrigation events were applied, corresponding to 180 mm of AIW. Irrigation management in the surrounding vineyard area was identical to that applied in the lysimeter zone.

The four radiation balance components (incoming and outgoing shortwave and longwave radiation) were monitored using an NR01 radiometer (Hukseflux, The Netherlands) positioned 4.5 m above ground level at the lysimeter site. Soil heat flux was measured by means of two heat flux plates (HFP01SC, Hukseflux, The Netherlands) installed at a depth of 8 cm. In order to estimate heat storage in the soil layer located above the plates, soil temperature was monitored at depths of 2 cm and 4 cm using thermocouples (TCAV, Type E, Campbell Sci. Inst., Shepshed, UK), while soil moisture content was recorded with a volumetric water content sensor (CS650, Campbell Sci. Inst., UK). The heat flux plates were

installed inside the lysimeter perimeter, one on each side of the east–west vine row and at a distance of 75 cm from the vines, so as to account for canopy influence and shading effects.

A total of five thermal infrared radiometers (SI-121, Apogee Instruments Inc., Logan, UT, USA) were deployed: two mounted on a mast located at the center of the row, two installed adjacent to the lysimeter area, and one directed upward. Radiometric temperature measurements were corrected for emissivity and atmospheric influences by applying the radiative transfer equation adapted for ground-based observations [26]. The upward-facing instrument provided measurements that were converted into radiance values and subsequently used as downwelling sky radiance for atmospheric correction procedures.

The turbulent fluxes were measured by an eddy covariance system (CSAT3, Campbell Sci. Inst., Logan, UT, USA and LI-7500, LI-COR Inc., Lincoln, NE, USA) deployed at 2.5 m in 2014 and at 3.5 m in 2015. The air temperature and humidity (MP100, Campbell Scientific Instrument, Logan, UT, USA), wind speed (A100R, Vector Instruments Ltd., Rhyl, UK), and wind direction (W200P, Vector Instruments Ltd., Rhyl, UK) were taken at the EC level. The manufacturer's recommendation was that the EC instruments should be deployed at a height above the canopy of at least 2–3 times the displacement height, and in any case never at less than 2 m above the top of the vegetation [27]. However, the latter would entail a footprint beyond the vineyard boundaries. The footprint analysis [28] showed that 90% of cumulative normalized flux measurements were obtained at an average of 48 $\pm$ 4 m and 76 $\pm$ 11 m distance upwind in 2014 and 2015, respectively. Figure 1 shows a plot of the vineyard and the average footprint for the different wind directions. The footprint fits within the vineyard field boundary for the whole dataset. Standard quality control and preprocessing procedures were applied before the fluxes were used in the analysis, including despiking, coordinate rotation, frequency response corrections, and filtering of low-quality data under insufficient-turbulence conditions [7].

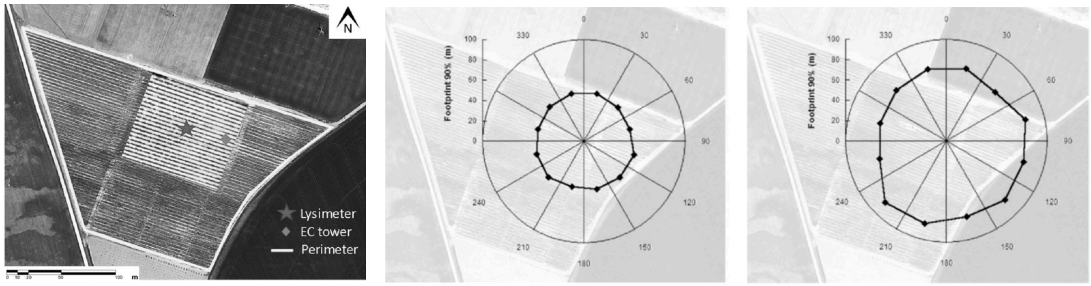

Figure 1. Overview of vineyard and perimeter. Lysimeter and eddy covariance tower emplacements marked with a star and a diamond, respectively (**left**). Average footprint as a function of the wind direction for 2014 (**middle**) and 2015 (**right**). Plots centered in the eddy covariance tower. Adapted from [7].

Digital photographic images were used to estimate the fractional vegetation cover (f_c) every week [29]. The plant height remained stable around 1.50 m, and f_c ranged from 0.25 to a maximum of 0.40.

Good agreement was reported between modeled and measured net radiation values, with an RMSE lower than 30 W m^{-2} and a bias of 10 W m^{-2} and $-$25 W m^{-2} for 2014 and 2015, respectively [7]. Average uncertainty for modeled soil heat flux was lower than $\pm$30 W m^{-2} with a bias below 20 W m^{-2} for both years.

2.1.2. A Young Almond Orchard

The experiment was conducted from 16 June to 16 October 2017 in a young almond orchard of *Prunus dulcis* (Mill.) D.A. Webb located at the Technical Institute of Agronomy Research Facility in Albacete (39°20 N, 2°50 W, 695 m a.s.l.) (Figure 2). The soil, classified as

Petrocalcic Calcixerepts, contained organic matter, nitrogen, and active limestone content of 1.55%, 0.09%, and 12.1%, respectively. The soil texture corresponded to a loam composition, including 31.6% sand, 42.4% silt, and 26% clay, and it showed a basic pH value of 8.4 [30].

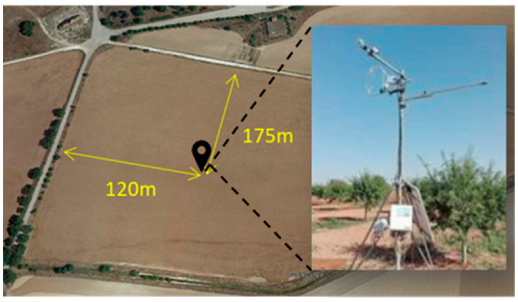

Figure 2. Meteorological and flux tower located in the almond orchard. Adapted from [25].

Average cumulative precipitation between March and November was 143 mm. The experimental period encompassed the complete Stage III phenological phase (seed weight increase) as well as a substantial part of Stages II (embryo growth) and IV (post-harvest). The orchard, covering 11 ha, was established in 2015 with a spacing of 6 m between trees and 7 m between rows, corresponding to a planting density of 238 trees ha^{-1}. Mean tree height was approximately 2.5 m. Irrigation was supplied through a drip irrigation system equipped with 3.2 L h^{-1} emitters placed every 0.75 m along the row, following the conventional irrigation management practices of the region. Irrigation scheduling was based on the soil water balance methodology, estimating crop water requirements following the FAO56 procedure [21,30].

Throughout the growing season, measurements were conducted weekly to determine canopy horizontal diameters and tree height, with the objective of modeling the fraction of green vegetation cover (fc). Minimum and maximum fc values were recorded around mid-May and late September, respectively, with values ranging from 0.1 to 0.2.

Sensible and latent heat fluxes were computed at half-hour intervals. The flux tower was equipped with a net radiometer (NR01, Hukseflux, The Netherlands), air temperature and relative humidity sensors (MP100, Campbell Scientific Instrument, Logan, UT, USA), and an eddy covariance system composed of a sonic anemometer (CSAT3, Campbell Sci. Inst., Logan, UT, USA) and an infrared gas analyzer (LI-7500, LI-COR Inc., Lincoln, NE, USA) operating at a frequency of 10 Hz. Wind speed and wind direction were obtained from the sonic anemometer measurements. All instruments were installed at a height of 4 m above ground level.

Soil and canopy albedo were derived from incoming and reflected solar radiation measurements obtained with the four-component net radiometer. Emissivity values for both soil and canopy were determined using the temperature–emissivity separation method [31] with a CIMEL CE-312-2 multispectral thermal radiometer (Cimel Electronique, Paris, France).

The flux tower also incorporated between two and four soil heat flux plates (HFP01SC, Hukseflux, The Netherlands) installed at 8 cm depth on both sides of the tree row. Soil temperature was measured at depths of 2 and 4 cm using thermocouples (TCAV, Type E, Campbell Sci. Inst., UK), while soil water content was monitored with volumetric moisture sensors (CS650, Campbell Sci. Inst., UK) to estimate heat storage in the soil layer located above the plates. Continuous thermal monitoring of soil and canopy temperatures was performed using three thermal infrared radiometers (SI-121, Apogee Instruments Inc., USA) mounted on the flux tower. Two radiometers were oriented downward at an angle of 45°, one targeting the canopy top and the other the inter-row soil surface, while the third

instrument was directed upward to measure downwelling sky radiance for atmospheric correction of canopy and soil temperature observations.

The flux tower was installed within the internal boundary layer depth, approximately in the center of the orchard (Figure 2). Eddy covariance instruments were aligned with the prevailing westward streamwise flow and positioned at a height of 1.5 m above the canopy to minimize the influence of adjacent areas outside the orchard boundaries. Footprint analysis [28] indicated that 90% of the cumulative normalized flux originated from average upwind distances of 178 ± 23 m [25]. These distances became considerably shorter when only unstable atmospheric conditions were considered. Standard preprocessing and quality control procedures previously described for the EC dataset were likewise applied in this study.

3. Theory

For unstable thermal stratification of the atmospheric surface layer, an ideal parallel scheme of the SR process is illustrated in Figure 3. Over 30 min, the model assumes the regular motion of a mean coherent structure in which a fresh macro-parcel of air, uniformly heated at a temperature T, descends to the ground to renew the previous one. A macro-parcel of air is defined as a parcel that covers all the sources whose volume (per unit surface) is Z (m^3) (Z is the measurement height). After a quiescent period, it is warmed while remaining in contact with the surface and subsequently, by continuity, another fresh macro-parcel of air sweeps across the surface replacing the previous one. The duration of the coherent motion, while the macro-parcel of air is in contact with the surface, is denoted by τ. The warming of the macro-parcel of air is not homogeneous, as it depends on the soil (T_s) and vegetation (T_c) temperature and is thus divided into two sub-parcels. The mean net temperature increase for the macro sub-parcels in contact with the soil and the vegetation during τ is denoted by A_s and A_c, respectively. It was shown that A_s and A_c were associated with ($T_s - T$) and ($T_c - T$), respectively [32–35]. When the macro sub-parcels of air are ejected upwards (i.e., attached to their corresponding macro parcel of air), turbulence rapidly mixes the air of the two macro sub-parcels of air, which represents an injection of sensible heat into upper air layers.

3.1. Background

3.1.1. Estimating the Sensible Heat Flux in Homogeneous Vegetation

The sensible heat flux can be estimated in the inertial layer as follows [34,35]:

$$H_C = \rho C_p \left(\frac{4k}{\pi\lambda}\right)^{1/2} \frac{\left(zh{\varphi_h}^{-1}\right)^{1/2} k u_*}{Z\left(ln\frac{z}{z_{0h}}\right)} (T_c - T) \quad (1)$$

In Equation (1), ρ and C_p are the density and isobaric heat capacity of the air, respectively; k is the Von Kármán constant (k = 0.4); z is the measurement height above the zero-plane displacement (d), $z = Z - d$, h is the canopy height; z_{0h} is the surface roughness length for heat; λ is a coefficient that depends on the atmospheric stability (0.5 and to 2/3 for unstable and stable conditions, respectively); u_* is the friction velocity; and φ_h is the stability correction function for heat transfer evaluated at z/L (L is the Obukhov length, $L = -\frac{u_*^3}{kgH}\rho C_p T$ with g being the gravity). Expressions to evaluate φ_h, u_* and z_{0h} are provided in Appendix A. The latter requires the wind measured at the reference height, u, and assumes the wind log-law profile.

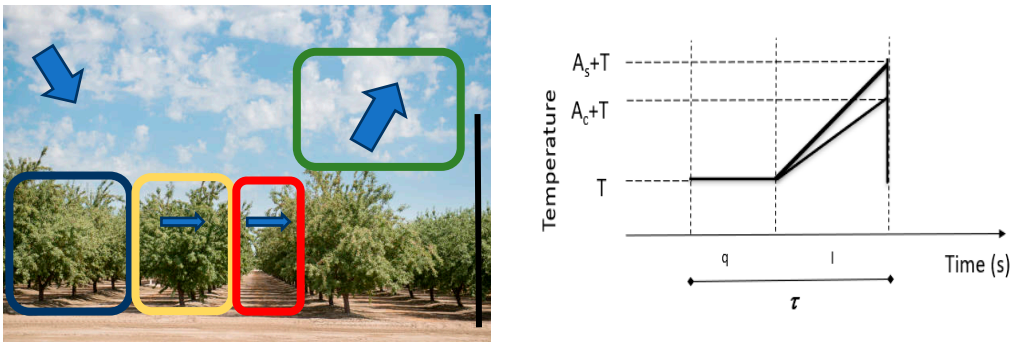

Figure 3. For an unstable case, the surface renewal (SR) model assumes that the two sources act independently (parallel scheme). From a Lagrangian perspective, SR analysis focuses on the role of a coherent structure (*CS*) ((**left**); the blue arrows denote the motion of a macro-parcel of air). By measuring the mean temperature of the macro-parcel air while it is in contact with the surface for a period τ, the signature of the *CS* is modeled as a ramp (**right**) representing the changing temperature of the macro-parcel air (vertical axis) with time (horizontal axis). The period τ is split into the quiescent period (q) and the warming period (l). During the warming period, the macro-parcel of air is divided into two sub-parcels of air. One reaches the vegetation temperature (yellow) with an amplitude $A_{C,}$ and the other reaches the soil temperature (red) with an amplitude $A_{S.}$ The amplitude A_C is associated with ($T_C - T_q$), and A_S is associated with ($T_S - T_q$), where T_C, T_S and T_q represent the vegetation, soil and the initial mean temperature of the macro-parcel of air during the q period, respectively. Next, the macro-parcel of air ejects, and the turbulence mixing make the temperature homogeneous (green), representing an injection of sensible heat flux measured at the height Z.

3.1.2. Estimating the Sensible Heat Flux from Bare Soils

The following expression was derived for estimating the sensible heat flux [24].

For unstable conditions,

$$H_s = \rho C_p \left(0.21\left(\frac{g\, z_{0h_s}}{T}\right)^{1/3} u\right)^{3/5} \left(\frac{(T_s - T)}{ln\left(\frac{Z}{z_{0h_s}}\right)}\right)^{6/5} \quad (2)$$

where z_{0h_s} is the surface roughness length for heat of the soil.

For stable conditions,

$$H_s = \rho C_p \left(0.11\varphi_h^{-1}\right)^{1/2} u_* \left(\frac{T_s - T}{ln\left(\frac{Z}{z_{0h_s}}\right) - \Psi_h}\right) \quad (3)$$

where Ψ_h is the integrated stability correction function for heat transfer (Appendix A).

Regardless of the stability conditions, z_{0h_s} was estimated as $z_{0h_s} = z_{0m_s} e^{-2}$ with z_{0m_s} being the surface roughness length for momentum of the soil evaluated in neutral conditions.

3.2. The STSEB Model

Based on the parallel approach [26,36], an STSEB model using the measured temperature of the canopy and the soil as inputs was proposed. The partitioning of the surface fluxes was as follows.

The partitioning of the net radiation flux between the soil and canopy was proposed:

$$R_n = f_c\, R_{nc} + (1 - f_c) R_{ns} \quad (4)$$

where R_{nc} and R_{ns} are the contributions of the canopy and soil, respectively, to the total net radiation flux, and f_c is the fractional vegetation cover. Establishing a balance between the

long-wave and short-wave radiation separately for each component, they were determined as follows:

$$R_{nc} = (1 - \alpha_c)S + \varepsilon_c L_{sky} - \varepsilon_c \sigma T_c^4 \quad (5)$$

$$R_{ns} = (1 - \alpha_s)S + \varepsilon_s L_{sky} - \varepsilon_s \sigma T_s^4 \quad (6)$$

where S is the solar global radiation (W m^{-2}); α_s and α_c are soil and canopy albedos, respectively; σ is the Stefan–Boltzmann constant; L_{sky} is the incident long-wave radiation (W m^{-2}); and ε_s and ε_c are the soil and the canopy emissivity.

The heat flux at the ground was estimated as follows [37]:

$$G = CG\, R_{ns} \quad (7)$$

where CG is an empirical parameter depending on the soil type and on the time of day. Thus, the available net surface flux ($R_n - G$) was estimated using Equations (4)–(7), $(R_n - G)_{Est}$.

The total latent heat flux was partitioned as

$$LE = f_c\, LE_c + (1 - f_c)LE_s \quad (8)$$

where LE_c is the contribution of the canopy, and LE_s is that of the soil. The latter were determined as follows:

$$LE_c = (R_{nc} - H_c) \quad (9)$$

$$LE_s = (R_{ns} - H_s) - G/(1 - f_c) \quad (10)$$

LE was converted to vineyard ET in (mm h^{-1}) by dividing by the latent heat of water vaporization, L (J kg^{-1}).

The soil and canopy albedo and the emissivity were set to $\alpha_s = 0.18$, $\alpha_c = 0.23$, $\varepsilon_s = 0.955$ and $\varepsilon_C = 0.985$. For this site, the recommended values of CG were 0.35 for daytime and 1.1 for nighttime [7].

4. Results and Discussion

Linear regression analysis was applied to compare estimated and reference values, including evaluation of the slope, intercept, and coefficient of determination (R^2). In addition, the root mean square error (RMSE) and the index of agreement (IA) were calculated. The index of agreement [38] is a standardized and dimensionless statistical indicator used to quantify model prediction error. Its values range from 0 to 1, with higher values indicating a stronger agreement between simulated and observed data. The uncertainties of CSAT3 and LI-7500 in measuring sensible heat flux and latent heat flux are ±20 W m^{-2} and ±35 W m^{-2}, respectively [16,39]. Accounting for other potential errors of measurement, intercepts below ±25 W m^{-2} and ±40 W m^{-2}, respectively, can be considered negligible.

4.1. Vineyards

Table 1 shows the linear regression parameters, RMSE, and IA used to compare the estimates and the reference values (H_{EC} and ET_{Lys}, respectively). Figures 4 and 5 show the performance of the modeled H_{SR} and $ET_{SR\text{-}RE}$ versus the reference for both years.

Table 1. Statistics from the linear regression analysis (slope, intercept (int.) and the coefficient of determination, (R^2), RMSE and the index of agreement (IA) comparing the modeled hourly sensible heat flux and evapotranspiration against the H_{EC} and ET_{Lys}, respectively, for 2014 and 2015. N is the number of data available.

2014	Slope	Int.	R^2	RMSE	IA	2015	Slope	Int.	R^2	RMSE	IA
N = 991		**(Wm^{-2})**		**(Wm^{-2})**		**N = 1210**		**(Wm^{-2})**		**(Wm^{-2})**	
H_{SR}	0.84	24	0.78	43	0.93		0.51	5	0.73	60	0.83
H_{MOST}	1.14	−9	0.60	56	0.84		0.54	−11	0.60	72	0.78
		(mm h^{-1})		(mm h^{-1})				(mm h^{-1})		(mm h^{-1})	
ET_{SR-RE}	0.92	−0.01	0.68	0.093	0.89		0.96	0.02	0.65	0.096	0.88
ET_{EC-RE}	1.06	−0.02	0.74	0.089	0.92		0.99	0.01	0.67	0.094	0.89
$ET_{MOST-RE}$	1.02	−0.04	0.67	0.108	0.88		1.01	0.00	0.65	0.098	0.88

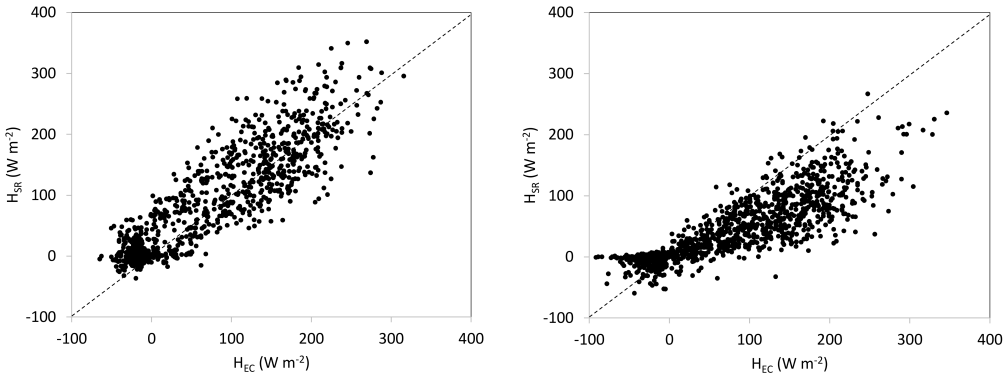

Figure 4. H_{SR} vs. H_{EC}, for 2014 (**left**) and 2015 (**right**) in the vineyard.

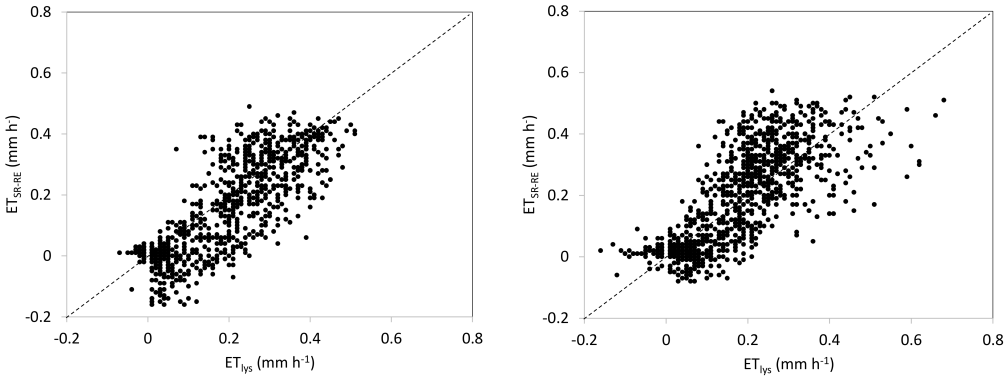

Figure 5. ET_{SR-RE} vs. ET_{Lys} for 2014 (**left**) and 2015 (**right**) in the vineyard.

For 2014, good performance was observed for H_{SR}, with a linear regression slope close to unity (0.98 when forced to the origin), a negligible intercept, a coefficient of determination R^2 = 0.78, and an RMSE value of 43 Wm^{-2}. For 2015, however, H_{SR} clearly underestimated H_{EC} (near 50%). This was partly a consequence of the hourly wind speed regime. The SR method relies on the existence of coherent turbulent structures. Under very low wind speeds (near-calm, stable conditions), these structures may be too weak. Figure 6 shows the wind speed frequency for intervals of 1 m/s. The number of samples for wind speeds exceeding 1 m/s was, in general, higher for 2014 than for 2015. For homogeneous canopies, it has been reported that SR analysis requires a wind threshold of approximately 0.7 m/s to achieve adequate air mixing, [40]; otherwise, it tends to underestimate the EC sensible heat flux under near-calm conditions. In comparison with H_{MOST}, slightly better performance was obtained with the SR approach (Table 1). The poorest results were obtained for 2015, where the RMSE and the IA were 72 Wm^{-2} and 78% using H_{MOST}. Focusing on the RMSE, H_{SR} performance under unstable conditions yielded values of 47 Wm^{-2} in 2014 and 70 Wm^{-2} in 2015, improving the results for H_{MOST} (58 Wm^{-2} and 84 Wm^{-2} for 2014

and 2015, respectively). For stable conditions, results were worse for both H_{SR} and H_{MOST} due to the overall low values registered under these conditions (Figure 4) and because of the wind speed regime. For stable conditions, 24% and 43% of the samples exhibited wind speeds lower than 1 m/s in 2014 and 2015, respectively. Overall (regardless of the year) according to the IA, the modeled H_{SR} shows better agreement with the observations than H_{MOST} (Table 1).

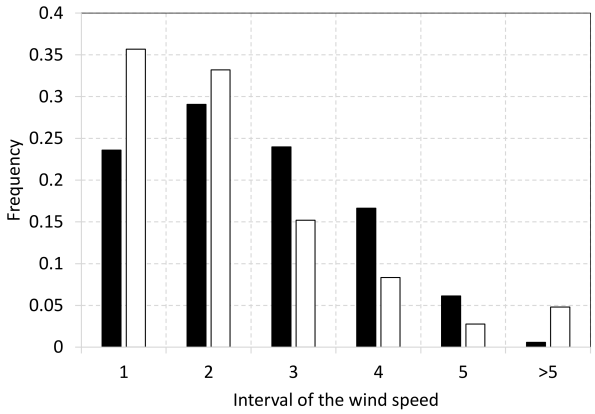

Figure 6. Hourly wind speed frequency for intervals of 1 m s^{-1} for 2014 (black) and 2015 (white).

Regardless of wind regime (Figure 6), the reasons for the better performance of H_{SR} in 2014 are not fully clear. Arguably, given that the soil sensible heat flux component dominates for irrigated crops, the estimation of the surface roughness length for soil heat needed adjustment. For example, raising the soil surface roughness length for momentum (z_{0m_s}) from 0.004 to 0.008, the sensible heat flux increases by 1.3%. This means that the slope, intercept and the coefficient of determination of the linear regression analysis would be 0.67, 7 Wm^{-2}, and 0.73, respectively, with an RMSE of 2 Wm^{-2} and an IA 83%. The z_{0m} is a property of the surface; therefore, perhaps the soil roughness was modified due to the technicians' practices around the lysimeter and to the soil moisture. Disregarding the sensible heat flux for stable conditions, for which the sensible heat estimates are generally unreliable due to the low wind speed values, for a variety of bare soils and assuming neutral conditions (setting z_{0m_s} = 0.004), H_{SR} performed better than H_{MOST}, given that the latter required site-specific calibration of kB^{-1} ($=ln\left(\frac{z_{0m}}{z_{0h}}\right)$) [24].

Regardless of the year, the linear regression analysis showed that $ET_{SR\text{-}RE}$ slightly tended to underestimate ET_{Lys} (Figure 5). Table 1 shows that the slope and the intercept were relatively close to 1 and 0, respectively, and a similar performance was observed compared to $ET_{EC\text{-}RE}$ and $ET_{MOST\text{-}RE}$. The highest determination coefficient was obtained for $ET_{EC\text{-}RE}$ (R^2 = 0.74) in 2014, with values for the other cases ranging between 0.65 and 0.68 (Table 1). In terms of RMSE, the best results were observed for $ET_{EC\text{-}RE}$.

The comparison between $ET_{SR\text{-}RE}$ and $ET_{MOST\text{-}RE}$ was slightly better for $ET_{SR\text{-}RE}$ (RMSE values of 0.093 mm h^{-1} and 0.096 mm h^{-1} for 2014 and 2015, respectively) than $ET_{MOST\text{-}RE}$ (0.108 mm h^{-1} and 0.098 mm h^{-1} for 2014 and 2015, respectively). However, regardless of the year, the index of agreement for SR and MOST was not conclusive, as all the IA values were close (Table 1) because of the lower sensible heat flux with respect to $(R_n - G)_{Est}$.

4.2. Almond Orchard

4.2.1. Energy Balance Closure

Table 2 shows the results of the linear regression analysis, RMSE and IA comparing (H_{EC} + LE_{EC}) and $(R_n - G)_{Est}$ with the actual ($R_n - G$). The coefficient of determination was 0.82, and the slope was close to unity (0.93). The RMSE resulted in 57 W m^{-2} and

an IA of 0.94. These results are consistent with those reported in the literature for sparse canopies [41,42]. Therefore, the energy balance closure was strong, lending credence to the EC sensible heat and the latent heat fluxes.

Table 2. Linear regression analysis (slope, intercept (Int.) and R^2), RMSE and the index of agreement (IA) comparing the turbulent fluxes (H_{EC} + LE_{EC}) and the available energy $(R_n - G)_{Est}$ against the actual $(R_n - G)$. N is the number of data, the intercept (Int.) and RMSE are expressed in W m^{-2} and the IA in %.

	Slope	Int.	R^2	RMSE	IA
N = 1164. (H_{EC} + LE_{EC}) vs. ($R_n - G$)	0.93	−11	0.82	57	94
$(R_n - G)_{Est}$ vs. ($R_n - G$)	0.99	−36	0.93	50	95

Figure 7 compares $(R_n - G)_{Est}$ with the actual $(R_n - G)$. Linear regression showed good agreement, with a slope of 0.99, an intercept of −36 W m^{-2}, and a coefficient of determination of 0.93. The RMSE was 50 W m^{-2}, and the IA was 0.95.

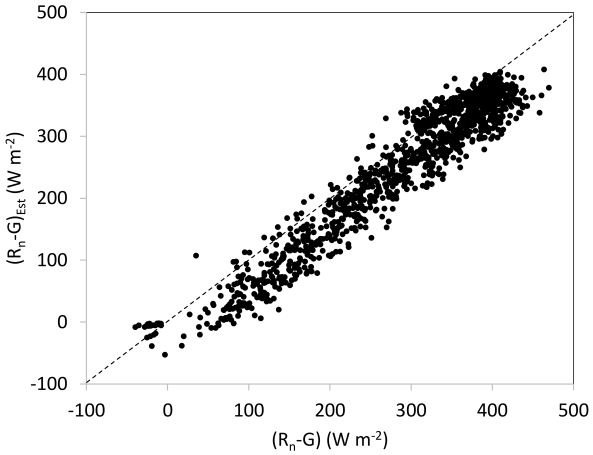

Figure 7. Modeled net surface energy, $(R_n - G)_{Est}$, with (Rn − G).

4.2.2. Turbulent Fluxes, H and LE

Table 3 shows the results of the linear regression analysis, RMSE and IA comparing the turbulent fluxes. H_{SR} performed slightly better than H_{MOST} (Figure 8). The former presented the strongest correlation (R^2 was 0.80 vs. 0.75) and slope closer to 1 (1.05 vs. 0.85). The RMSE was 43 W m^{-2} and 46 W m^{-2} for SR and MOST, respectively, and the index of agreement was slightly higher for SR than MOST (93% vs. 90%).

Table 3. Linear regression analysis (slope, intercept (Int.) and R^2), RMSE and the index of agreement (IA) comparing the H_{SR} and H_{STSEB} against H_{EC}, LE_{SR} and LE_{MOST} with LE_{EC}, and $LE_{SR\text{-}RE}$ and $LE_{MOST\text{-}RE}$ against $((R_n - G)_{Est} - H_{EC})$. The intercept and RMSE are expressed in W m^{-2} and the IA in %.

	Slope	Int.	R^2	RMSE	IA
H_{SR}	1.05	−24	0.80	43	93
LE_{SR}	0.67	48	0.36	71	77
$LE_{SR\text{-}RE}$	0.90	−6	0.66	48	81
H_{MOST}	0.85	−6	0.75	46	90
LE_{MOST}	0.60	64	0.33	71	75
$LE_{MOST\text{-}RE}$	0.77	24	0.61	49	78

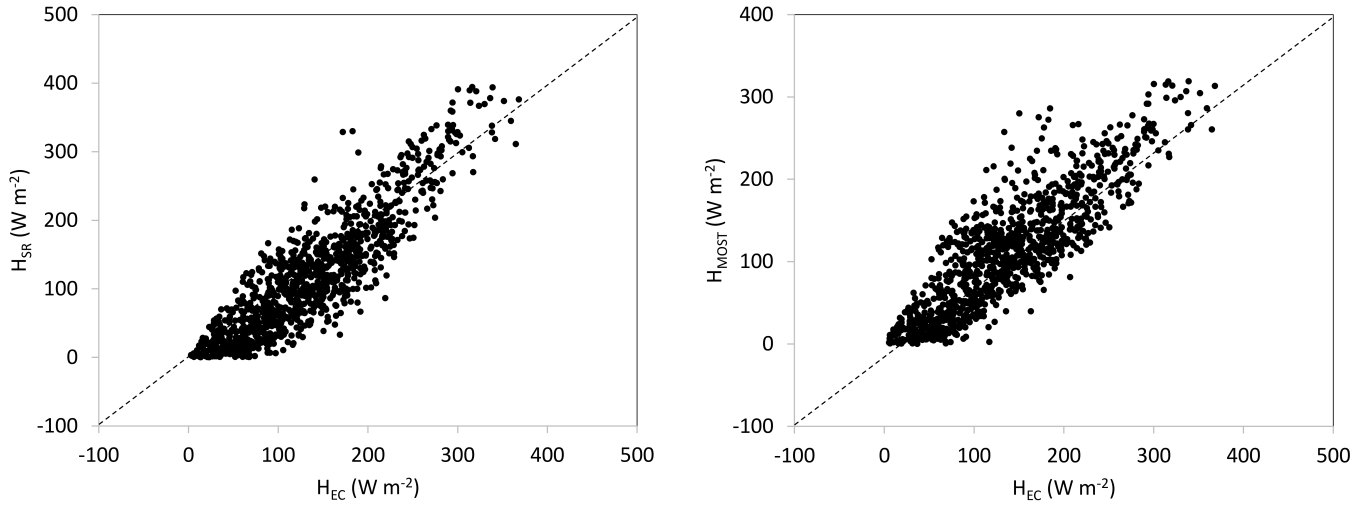

Figure 8. H_{SR} (**left**) and H_{MOST} (**right**) with the reference.

For latent heat flux, when comparing the performances of SR and SR-RE obtained vs. their respective references, the SR-RE method demonstrated better performance (Table 2). Comparing SR-RE vs. SR, we obtained a coefficient of determination of 0.66 vs. 0.36, and a slope closer to 1, 0.90, vs. 0.67. For SR-RE, the intercept was negligible, while for SR, it was 48 W m^{-2}. Additionally, RMSE was 48 W m^{-2} vs. 71 W m^{-2}, and the index of agreement was 81% vs. 77%.

Comparing the performances of $LE_{MOST\text{-}RE}$ and LE_{MOST} vs. their respective references, all the statistics were better for $LE_{MOST\text{-}RE}$ than for LE_{MOST}. Moreover, both LE_{SR} and $LE_{SR\text{-}RE}$ were slightly superior to LE_{MOST} and $LE_{MOST\text{-}RE}$, respectively (Table 2). Figure 5 compares the latent heat flux estimates for $LE_{SR\text{-}RE}$ against reference values. The differences between $LE_{SR\text{-}RE}$ and $LE_{MOST\text{-}RE}$ were small because of the large value of $(R_n - G)_{Est}$ in comparison with sensible heat flux.

5. Conclusions

The simplified original Two-Source model based on MOST for estimating the turbulent fluxes was applied using a parallel scheme based on Ohms's law, in which soil and canopy temperatures, together with all the meteorological data and biophysical information, were available [7,24,25,36]. An SR-based method to partition the turbulent fluxes was tested and compared with the MOST approach. The partition of the net radiation, the soil heat flux, and the evapotranspiration remained the same as the original method. The required inputs were the same for SR and MOST. In vineyards, the hourly sensible heat flux (H) and the evapotranspiration (ET) measured with the eddy covariance system (EC) and with the lysimeter, respectively, were used as a reference. Evapotranspiration was estimated using the residual method (RE). Regardless of the wind regime, the comparison with H_{EC} showed that H_{SR} slightly improved H_{MOST}. The index of agreement was 93% vs. 84% in 2014, and 83% vs. 78% in 2015 for H_{SR} and H_{MOST}, respectively. $ET_{SR\text{-}RE}$ performed comparably to $ET_{MOST\text{-}RE}$. For the almond orchard's SR sensible heat flux, performance was slightly better than MOST, showing an IA of 93% vs. 90% for SR and MOST, respectively. For estimation of latent heat flux, the performance was not statistically significant using either LE_{SR} or LE_{MOST}. For the residual method, $LE_{SR\text{-}RES}$ performed slightly better than $LE_{MOST\text{-}RES}$ ($IA_{SR\text{-}RES}$ = 81% and $IA_{MOST\text{-}RES}$ = 78%). Recalling that the EC method is used for research purposes, SR appears to be a feasible alternative. Overall, this work shows that, for both drip-irrigated grapevines and young almond trees in a semi-arid climate, SR

performs comparably to (or slightly improves) the MOST method. However, SR was not consistently superior.

Author Contributions: J.M.S. and R.L.-U. designed the research and assisted with processing of data for analysis; F.C. conducted the surface renewal analysis; J.M.S. and R.L.-U. carried out the STSEB analysis and collected the lysimeter and EC data; F.C. wrote the manuscript; J.M.S. and R.L.-U. reviewed and edited the manuscript. All authors have read and agreed to the published version of the manuscript.

Funding: This work is part of the research project PID2021-124006OB-I00 funded by MCIN/AEI/10.13039/501100011033 and by the European Regional Development Fund (ERDF A way of making Europe).

Institutional Review Board Statement: Not applicable.

Informed Consent Statement: Not applicable.

Data Availability Statement: The original contributions presented in this study are included in the article. Further inquiries can be directed to the corresponding author.

Acknowledgments: The authors gratefully acknowledge the logistic support of ITAP technicians in the instrumentation maintenance. This work is part of the research projects PID2021–123305OB-C31 and PID2024-161881OB-C21.

Conflicts of Interest: The authors declare they have no competing interests.

Appendix A. Similarity Functions

The following expressions were used to determine the similarity functions [8,43] in Equation (1).

The wind log-law was used to estimate the friction velocity from the horizontal mean wind speed measured at the reference height (u):

$$u_* = \frac{ku}{\ln \frac{z}{z_{0m}} - \Psi_{m(z/L)} + \Psi_{m(z_{0m}/L)}} \quad \text{(A1)}$$

where k is the Von Kármán constant (k = 0.4), z is the measurement height above the zero-plane displacement (d), $z = Z - d$, z_{0m} is the surface roughness length for heat for momentum, L is the Obukhov length, and Ψ_m is the integrated stability function for momentum transfer. For unstable conditions,

$$\Psi_m(x) = 2\ln(0.5(1+x)) + \ln\left(0.5\left(1+x^2\right)\right) - 2atang(x) + 0.5\pi \quad \text{(A2)}$$

where $x = \left(1 - 16\frac{z}{L}\right)^{\frac{1}{4}}$.

For stable conditions,

$$\Psi_m = 5\, z/L \quad \text{(A3)}$$

φ_h is the stability correction function for heat transfer. For unstable conditions,

$$\varphi_h = \left(1 - 16\frac{z}{L}\right)^{-1/2} \quad \text{(A4)}$$

For stable conditions,

$$\varphi_h = \left(1 + 5\frac{z}{L}\right) \quad \text{(A5)}$$

And the integrated φ_h is

$$\Psi_h = 5z/L \quad \text{(A6)}$$

z_{0m} was estimated as $0.125h$ (h is the canopy height), and the surface roughness length for heat transfer, z_{0h}, was estimated as, $z_{0h} = z_{0m}e^{-2}$ [44]. The zero-plane displacement was estimated as $2/3h$. For bare soil, z_{0m_s} was set to 0.004 m.

References

1. Howell, T.A.; Steiner, J.L.; Schneider, A.D.; Evett, S.R. Evapotranspiration of irrigated winter wheat: Southern high plains. *Trans. ASAE* **1995**, *38*, 745–759. [CrossRef]
2. Anderson, M.C.; Allen, R.G.; Morse, A.; Kustas, W.P. Use of Landsat thermal imagery in monitoring evapotranspiration and managing water resources. *Remote Sens. Environ.* **2012**, *122*, 50–65. [CrossRef]
3. Anderson, M.C.; Kustas, W.P.; Norman, J.M. A brief history of the thermal IR-based Two-Source Energy Balance (TSEB) model—Diagnosing evapotranspiration from plant to global scales. *Agric. For. Meteorol.* **2024**, *350*, 109951. [CrossRef]
4. Li, S.; Kang, S.; Zhang, L.; Li, F.; Zhu, Z.; Zhang, B. A comparison of three methods for determining vineyard evapotranspiration in the arid desert regions of northwest China. *Hydrol. Process.* **2008**, *22*, 4554–4564. [CrossRef]
5. Er-Raki, S.; Rodriguez, J.C.; Garatuza-Payan, J.; Watts, C.J.; Chehbouni, A. Determination of crop evapotranspiration of table grapes in a semi-arid region of Northwest Mexico using multi-spectral vegetation index. *Agric. Water Manag.* **2013**, *122*, 12–19. [CrossRef]
6. Campos, I.; Balbontín, C.; González-Piqueras, J.; González-Dugo, M.P.; Neale, C.M.U.; Calera, A. Combining a water balance model with evapotranspiration measurements to estimate total available soil water in irrigated and rainfed vineyards. *Agric. Water Manag.* **2016**, *165*, 141–152. [CrossRef]
7. Sánchez, J.M.; López-Urrea, R.; Valentín, F.; Caselles, V.; Galve, J.M. Lysimeter assessment of the Simplified Two-Source Energy Balance model and eddy covariance system to estimate vineyard evapotranspiration. *Agric. For. Meteorol.* **2019**, *274*, 172–183. [CrossRef]
8. Brutsaert, W.H. *Evaporation into the Atmosphere*, 1st ed.; Environmental Fluid Mechanics; Kluwer Academic Publishers: Dordrecht, The Netherlands; Boston, MA, USA; London, UK, 1982; pp. 1–400.
9. Kool, D.; Kustas, W.P.; Ben-Gal, A.; Agam, N. Energy partitioning between plant canopy and soil, performance of the two-source energy balance model in a vineyard. *Agric. For. Meteorol.* **2021**, *300*, 108328. [CrossRef]
10. Kool, D.; Agam, N.; Lazarovitch, N.; Heitman, J.L.; Sauer, T.J.; Ben-Gal, A. A review of approaches for evapotranspiration partitioning. *Agric. For. Meteorol.* **2014**, *184*, 56–70. [CrossRef]
11. Espadafor, M.; Orgaz, F.; Testi, L.; Lorite, I.J.; Villalobos, F.J. Transpiration of young almond trees in relation to intercepted radiation. *Irrig. Sci.* **2015**, *33*, 265–275. [CrossRef]
12. García-Tejero, I.F.; Hernández, A.; Rodríguez, V.M.; Ponce, J.R.; Ramos, V.; Muriel, J.L.; Durán-Zuazo, V.H. Estimating almond crop coefficients and physiological response to water stress in semiarid environments (SW Spain). *J. Agric. Sci. Technol.* **2015**, *17*, 1255–1266.
13. Bellvert, J.; Adeline, K.; Baram, S.; Pierce, L.; Sanden, B.L.; Smart, D.R. Monitoring crop evapotranspiration and crop coefficients over an almond and pistachio orchard throughout remote sensing. *Remote Sens.* **2018**, *10*, 2001. [CrossRef]
14. Kustas, W.P.; Alfieri, J.G.; Nieto, H.; Wilson, T.G.; Gao, F.; Anderson, M.C. Utility of the two-source energy balance (TSEB) model in vine and interrow flux partitioning over the growing season. *Irrig. Sci.* **2018**, *10*, 2001. [CrossRef]
15. Rallo, G.; Paço, T.; Paredes, P.; Puig, A.; Provenzano, G.; Massai, R.; Pereira, L.S. Updated single and dual crop coefficients for trees and vine crops. *Agric. Water Manag.* **2021**, *250*, 106645. [CrossRef]
16. Foken, T. The Energy Balance Closure Problem: An Overview. *Ecol. Appl.* **2008**, *8*, 1351–1367. [CrossRef]
17. Qi, Y.; Shang, X.; Chen, G.; Gao, Z.; Bi, Z.; Yu, Y.; Mao, H. Re-estimation of the vertical sensible heat flux by determining the environmental temperature on a single-point tower measurement. *Front. Earth Sci.* **2024**, *12*, 1269252. [CrossRef]
18. Allen, R.G.; Pereira, L.S.; Howell, T.A.; Jensen, M.E. Evapotranspiration information reporting: I. Factors governing measurement accuracy. *Agr. Water Manag.* **2011**, *98*, 899–920. [CrossRef]
19. Evett, S.R.; Schwartz, R.C.; Howell, T.A.; Baumhardt, R.L.; Copeland, K.S. Can weighing lysimeter ET represent surrounding field ET well enough to test flux station measurements of daily and sub-daily ET? *Adv. Water Resour.* **2012**, *50*, 79–90. [CrossRef]
20. López-Urrea, R.; Montoro, A.; Mañas, F.; López-Fuster, P.; Fereres, E. Evapotranspiration and crop coefficients from lysimeter measurements of mature "Tempranillo" wine grapes. *Agric. Water. Manag.* **2012**, *112*, 13–20. [CrossRef]
21. Pereira, L.S.; Allen, R.G.; Paredes, P.; López-Urrea, R.; Raes, D.; Smith, M.; Kilic, A.; Salman, M. *Crop Evapotranspiration—Guidelines for Computing Crop Water Requirements*, 2nd ed.; FAO Irrigation and Drainage Paper, No.56 Rev.1; FAO: Rome, Italy, 2025.
22. Castellví, F.; Gonzalez-Dugo, M.P. A series-scheme surface-renewal method within a two-source energy-balance framework. *Agric. For. Meteorol.* **2026**, *376*, 110903. [CrossRef]
23. Kustas, W.P.; Norman, J.M. Evaluation of soil and vegetation heat flux predictions using a simple two-source model with radiometric temperatures for partial canopy cover. *Agric. For. Meteorol.* **1999**, *94*, 13–29. [CrossRef]

24. Castellví, F.; Agam, N. A New Approach to Estimating the Sensible Heat Flux in Bare Soils. *Atmosphere* **2025**, *16*, 458. [CrossRef]
25. Sánchez, J.M.; Simón, L.; González-Piqueras, J.; Montoya, F.; López-Urrea, R. Monitoring Crop Evapotranspiration and Transpiration/Evaporation Partitioning in a Drip-Irrigated Young Almond Orchard Applying a Two-Source Surface Energy Balance Model. *Water* **2021**, *13*, 2073. [CrossRef]
26. Sánchez, J.M.; Kustas, W.P.; Caselles, V.; Anderson, M. Modelling surface energy fluxes over maize using a two-source patch model and radiometric soil and canopy temperature observations. *Remote Sens. Environ.* **2008**, *112*, 1130–1143. [CrossRef]
27. Burba, G. *Eddy Covariance Method for Scientific, Industrial, Agricultural, and Regulatory Applications: A Field Book on Measuring Ecosystem Gas Exchange and Areal Emission Rates*; LI-COR Biosciences: Lincoln, NE, USA, 2013; 331p.
28. Kljun, N.; Calanca, P.; Rotach, M.W.; Schmid, H.P. A simple parameterization for flux footprint predictions. *Bound. Layer Meteorol.* **2004**, *112*, 503–523. [CrossRef]
29. Cihlar, J.; Dobson, M.C.; Schmugge, T.; Hoogeboom, P.; Janse, A.R.P.; Baret, F.; Guyot, G.; Le Toan, T.; Pampaloni, P. Procedures for the description of agricultural crops and soils in optical and microwave remote sensing studies. *Int. J. Remote Sens.* **1987**, *8*, 427–439. [CrossRef]
30. Staff, S.S. *Keys to Soil Taxonomy*, 12th ed.; USDA-Natural Resources Conservation Service: Washington, DC, USA, 2014.
31. Sánchez, J.M.; French, A.N.; Mira, M.; Hunsaker, D.J.; Thorp, K.R.; Valor, E.; Caselles, V. Thermal Infrared Emissivity Dependence on Soil Moisture in Field Conditions. *IEEE Trans. Geosci. Remote Sens.* **2011**, *49*, 4652–4659. [CrossRef]
32. Castellví, F. Combining surface renewal analysis and similarity theory: A new approach for estimating sensible heat flux. *Water Resour. Res.* **2004**, *40*, W05201. [CrossRef]
33. Castellví, F.; Cammalleri, C.; Ciraolo, G.; Maltese, A.; Rossi, F. Daytime sensible heat flux estimation over heterogeneous surfaces using multitemporal land-surface temperature observations. *Water Resour. Res.* **2016**, *52*, 3457–3476. [CrossRef]
34. Castellví, F.; Oliphant, A.J. Daytime sensible and latent heat flux estimates for a mountain meadow using in-situ slow-response measurements. *Agric. For. Meteorol.* **2017**, *236*, 135–144. [CrossRef]
35. Castellví, F.; González-Dugo, M.P. A one–source model to estimate sensible heat flux in agricultural landscapes. *Agric. For. Meteorol.* **2021**, *310*, 108628. [CrossRef]
36. Norman, J.M.; Kustas, W.; Humes, K. A two-source approach for estimating soil and vegetation energy fluxes from observations of directional radiometric surface temperature. *Agric. For. Meteorol.* **1995**, *77*, 263–293. [CrossRef]
37. Choudhury, B.J.; Idso, S.B.; Reginato, R.J. Analysis of an empirical model for soil heat flux under a growing wheat crop for estimating evaporation by an infrared-temperature based energy balance equation. *Agric. For. Meteorol.* **1987**, *39*, 283–297. [CrossRef]
38. Willmott, C.J. Some comments on the evaluation of model performance. *Bull. Am. Meteorol. Soc.* **1982**, *63*, 1309–1313. [CrossRef]
39. Mauder, M.; Oncley, S.P.; Vogt, R.; Weidinger, T.; Ribeiro, L.; Bernhofer, C.; Foken, T.; Kohsiek, W.; de Bruin, H.A.R.; Liu, H. The Energy Balance Experiment EBEX-2000. Part II: Intercomparison of eddy-covariance sensors and post-field data processing methods. *Bound-Layer Meteorol.* **2007**, *123*, 29–54. [CrossRef]
40. Castellví, F.; Medina, E.; Cavero, J. Surface eddy fluxes and friction velocity estimates taking measurements at the canopy top. *Agric. Water Manag.* **2020**, *241*, 106358. [CrossRef]
41. Jofre-Čekalović, C.; Nieto, H.; Girona, J.; Pamies-Sans, M.; Bellvert, J. Accounting for Almond Crop Water Use under Different Irrigation Regimes with a Two-Source Energy Balance Model and Copernicus-Based Inputs. *Remote Sens.* **2022**, *14*, 2106. [CrossRef]
42. Souto, C.; Lagos, O.; Holzapfel, E.; Ruybal, C.; Bryla, D.R.; Vidal, G. Evaluating a Surface Energy Balance Model for Partially Wetted Surfaces: Drip and Micro-Sprinkler Systems in Hazelnut Orchards (*Corylus avellana* L.). *Water* **2022**, *14*, 4011. [CrossRef]
43. Dyer, A.J. A review of flux-profile relationships. *Bound-Layer Meteorol.* **1974**, *7*, 363–372. [CrossRef]
44. Crago, R.D.; Qualls, R.J. Use of land surface temperature to estimate surface energy fluxes: Contributions of Wilfried Brutsaert and collaborators. *Water Resour. Res.* **2014**, *50*, 3396–3408. [CrossRef]

Disclaimer/Publisher's Note: The statements, opinions and data contained in all publications are solely those of the individual author(s) and contributor(s) and not of MDPI and/or the editor(s). MDPI and/or the editor(s) disclaim responsibility for any injury to people or property resulting from any ideas, methods, instructions or products referred to in the content.